Full-Scale Turbofan Demonstration of a Deployable Engine Air-Brake for Drag Management Applications[1]

Parthiv N. Shah
ATA Engineering, Inc.,
San Diego, CA 92128
e-mail: parthiv.shah@ata-e.com

Gordon Pfeiffer
ATA Engineering, Inc.,
San Diego, CA 92128
e-mail: gordon.pfeiffer@ata-e.com

Rory Davis
ATA Engineering, Inc.,
San Diego, CA 92128
e-mail: rory.davis@ata-e.com

Thomas Hartley
Williams International,
Walled Lake, MI 48390
e-mail: THartley@williams-int.com

Zoltán Spakovszky
Massachusetts Institute of Technology,
Cambridge, MA 02139
e-mail: zolti@mit.edu

This paper presents the design and full-scale ground-test demonstration of an engine air-brake (EAB) nozzle that uses a deployable swirl vane mechanism to switch the operation of a turbofan's exhaust stream from thrust generation to drag generation during the approach and/or descent phase of flight. The EAB generates a swirling outflow from the turbofan exhaust nozzle, allowing an aircraft to generate equivalent drag in the form of thrust reduction at a fixed fan rotor speed. The drag generated by the swirling exhaust flow is sustained by the strong radial pressure gradient created by the EAB swirl vanes. Such drag-on-demand is an enabler to operational benefits such as slower, steeper, and/or aeroacoustically cleaner flight on approach, addressing the aviation community's need for active and passive control of aeroacoustic noise sources and access to confined airports. Using NASA's technology readiness level (TRL) definitions, the EAB technology has been matured to a level of six, i.e., a fully functional prototype. The TRL-maturation effort involved design, fabrication, assembly, and ground-testing of the EAB's deployable mechanism on a full-scale, mixed-exhaust, medium-bypass-ratio business jet engine (Williams International FJ44-4A) operating at the upper end of typical approach throttle settings. The final prototype design satisfied a set of critical technology demonstration requirements that included (1) aerodynamic equivalent drag production equal to 15% of nominal thrust in a high-powered approach throttle setting (called dirty approach), (2) excess nozzle flow capacity and fuel burn reduction in the fully deployed configuration, (3) acceptable engine operability during dynamic deployment and stowing, (4) deployment time of 3–5 s, (5) stowing time under 0.5 s, and (6) packaging of the mechanism within a notional engine cowl. For a typical twin-jet aircraft application, a constant-speed, steep approach analysis suggests that the EAB drag could be used without additional external airframe drag to increase the conventional glideslope from 3 deg to 4.3 deg, with about 3 dB noise reduction at a fixed observer location.
[DOI: 10.1115/1.4037155]

Introduction

Takeoff and approach are the two events responsible for aircraft community noise exposure. Takeoff is dominated by noise from the engine at high power, while on approach airframe noise competes with and often exceeds engine noise due to the aerodynamic exposure of structures such as landing gear, high-lift devices, control surfaces, and speedbrakes [1,2]. These structures all generate drag, which contributes to the aircraft's force balance—but their noise typically scales with flight speed to an exponent between 5 and 6. This motivates the need for "quiet" drag devices that may be deployed on approach to reduce noise through flight paths that are slower, aerodynamically cleaner, or steeper (thereby distancing the sound source from the community).

Operational methods to reduce community noise have come into focus in the last two decades [3], with significant effort placed on the development of steeper and/or slower descent and approach trajectories for noise reduction. Typical transport aircraft glideslopes are around 3 deg unless modified by local requirements, but steeper descent maneuvers and their potentially beneficial impact on noise have gained interest in recent years. Antoine and Kroo [4] estimated the noise reduction of a steep approach of 4.5 deg to be as much as 7.7 dB. Filippone simulated the A310 [5] and

determined that up to 6.0 dB noise reduction could be achieved from increases in both maximum lift and zero-lift drag, and he concluded that further investigation was needed into devices that increase the nonlifting portion of drag without affecting the high-lift system.

Aircraft noise is regulated *globally* by the International Civil Aviation Organization, but it is often increasing *local* requirements that dictate key elements of the design of aircraft for lower noise. Influential airport authorities will continue to push for enabling technologies for noise reductions. Significant successes on continuous-descent approaches (CDAs) [6,7] have brought these procedures into more frequent use. London Heathrow airport's 2015 "blueprint for noise reduction" [8] includes both a campaign for quiet approaches focused on CDAs and exploration of steeper angles of descent as two of its top ten practical steps to cut noise.

A quiet drag device may enable greater access to geographically confined airports. The 2006 Airbus A318 steep approach certification for London City Airport was developed for competitive advantage, allowing the aircraft to be marketed as a regional jet replacement [9]. The drag management procedure required simultaneous use of high-lift, high-drag flaps and lift-spoiling high-drag speed brakes, since neither device could generate sufficient drag alone. The resulting higher approach speed led to landings deemed "firmer than ideal." Today, British Airways flies the A318 in an all-business-class configuration between John F. Kennedy International Airport and London City Airport.

Recent work on drag devices for steep descent or approach applications has focused on the airframe [10–12], acknowledging

Table 1 Estimated $C_{d,\text{eq}}$ to change conventional 3 deg glideslope to 4 deg or 6 deg for several two-engine aircraft

Two-engine aircraft				3–4 deg (+1 deg)	3–6 deg (+3 deg)
Aircraft	Assumed V_{app} (m/s)	Assumed max. landing mass (kg)	Assumed total fan (circular) area (m^2)	−2.5 dB max under flight path Quiet $C_{d,\text{eq}}$	−6 dB max under flight path Quiet $C_{d,\text{eq}}$
CJ4	61.7	7031	0.64	0.80	2.41
G550	61.7	34,200	2.33	1.08	3.23
737-800	73.1	65,320	3.77	0.91	2.72
787-8	72.0	166,000	12.49	0.72	2.17

that to avoid increasing approach speed and thus adversely impacting noise and landing distance, drag generation should not degrade high-lift performance. Reducing landing distance (i.e., short-field performance) is a competitive advantage, particularly for business jets whose owners demand convenience [13].

The engine's thrust on approach opposes the additional drag being sought in these scenarios. A seemingly simple solution would be to propose to greatly reduce power to engines during approach, but this is constrained by the requirement of a minimum spool-up time to ensure safe go-around during aborted landings [14,15].

Additionally, during descent in icing conditions, engines also run at higher than normal fan rotor speeds (N1) to deliver anti-ice bleed air, and the associated excess thrust may lengthen the duration of descent and cause excess fuel burn. Such scenarios make energy management on descent an important topic, especially for low-drag aircraft such as modern business jets [16].

The present work is focused on drag generation through thrust reduction using a deployable—and rapidly stowable—device called an engine air-brake (EAB). A figure of merit for EAB performance is "equivalent drag," which is the engine net thrust reduction achieved by swirling the bypass stream exhaust. Equation (1) defines the equivalent drag coefficient as this thrust reduction at fixed N1, normalized by approach dynamic pressure and a reference area

$$C_{d,\text{eq}} = \left(\frac{\Delta F_n}{\frac{1}{2}\rho_\infty V_{\text{app}}^2 A_{\text{ref}}} \right)_{\text{Fixed } N1} \qquad (1)$$

Fixing of the fan rotor speed addresses the go-around requirement in the case of a missed approach, provided the device can be stowed on a timescale much shorter than the typical 8 s spool-up required in FAR 25 [14]. It also ensures that the anti-icing requirement is satisfied during descent in inclement weather.

Constant-speed, steep approach provides a simple way to assess quiet drag device impact. For small glideslope angles, θ, the force balance in the direction of flight equates the weight component ($W \sin\theta$) with the aircraft drag (D) minus engine net thrust (F_n). Assuming a fixed aircraft aerodynamic configuration, the airframe's baseline lift, drag, and noise remain unchanged. The small angle approximation gives $\sin\theta \approx \theta$, so doubling the aircraft's glideslope to an angle 2θ requires an additional component of drag (or thrust reduction) roughly equal to $W\theta$. So, for example, to perform a 6 deg approach at constant speed requires a drag addition of about 5% of the aircraft's landing weight relative to the 3 deg baseline. Assuming the additional drag required to fly the steep trajectory is quiet, this can lead to a lower perceived noise on the ground.

Table 1 summarizes the impact of quiet drag on four twin-engine aircraft, including two business jets (Cessna CJ4 and Gulfstream G550) and two commercial transports (737-800 and 787-8). For these aircraft, relative to a baseline 3 deg glideslope, a quiet $C_{d,\text{eq}}$ of 0.72–1.08 based on total fan circular area[2] enables a

+1 deg glideslope increase resulting in a maximum noise reduction of 2.5 dB below the flight path. Quiet drag coefficients of 2.17–3.23 enable a +3 deg glideslope change from 3 deg to 6 deg[3] with a corresponding maximum overall noise reduction of about 6 dB.

Background

Figure 1 presents a technology development roadmap for the development of the EAB that is discussed in this paper. As shown in the lower-left portion of the figure, generation of a swirling outflow from the engine's propulsion system to reduce approach thrust was originally proposed by Shah et al. [17–19]. Low-technology readiness level (TRL) proof of concept was demonstrated experimentally in a simple ram-pressure-driven nacelle with swirl vanes (a "swirl tube") to generate drag quietly. Testing in the MIT Wright Brothers wind tunnel demonstrated a maximum drag coefficient of about 0.8 based on through-flow area. Far-field noise measurements at the NASA Langley Quiet Flow Facility suggested a relatively imperceptible far-field noise signature of about 44 dBA when extrapolated to full scale (2.16 m diameter, 120 m).

An engine-integrated (i.e., fan-driven, or "pumped") swirl tube was next conceptually introduced by Shah et al. [17]. It was shown that such an EAB configuration would produce equivalent drag in the form of thrust reduction. The increased swirl vane loadings would result in higher $C_{d,\text{eq}}$, though the swirling wake would be replaced by a swirling jet with higher Mach numbers on the centerline and higher noise.

Next, a concept development program for two stream engine nozzles began with the development of design concepts and progressed to the design, implementation, and operation of several aerodynamic prototypes in NASA's Aero Acoustic Propulsion Laboratory. In quantifying the relationship between swirl, flow, drag, and noise, aircraft-on-approach noise simulations were used to demonstrate that an appropriately designed EAB could enable a steep approach trajectory (from a baseline 3.2 deg glideslope to 4.4 deg) for a 737-800–class aircraft at a fixed speed. A peak perceived noise level, tone (correction factor) (PNLT) reduction of up to 3.1 dB was predicted at the ground observer location, with a potential 1.8 dB effective perceived noise level (EPNL) reduction [20,21].

The concept development program culminated in a prototype paper design for a swirl vane deployment mechanism that would remain stowed and aerodynamically "invisible" to the bypass flow path during conventional operation and would then deploy a set of vanes projecting inward from the fan nozzle casing surface during drag management maneuvers. A conceptual design of this mechanism was explored as part of a system demonstration program using NASA's separate-flow 4BB nozzle geometry.

ATA collaborated with Williams International (WI), leading to the selection of the FJ44-4 A mixed-flow turbofan as the test article for demonstration. It powers the Cessna CJ4 and the Pilatus

---

[2]The targeted EAB drag levels are comparable to the zero-lift drag of these classes of aircraft. Using the wing area as a reference instead, the $C_{d,\text{eq}}$ range covers drag counts of 168–279 for a +1 deg glideslope change. These numbers may be multiplied by 3 for the +3 deg glideslope scenario.

[3]It should be noted that for the 6 deg constant-speed, steep-approach scenario, this analysis assumes sink rates in excess of 1100 ft/s, which may be a passenger comfort constraint (e.g., see Ref. [4].). For the 4 deg constant-speed, steep-approach scenario, sink rates do not exceed 1100 ft/s.
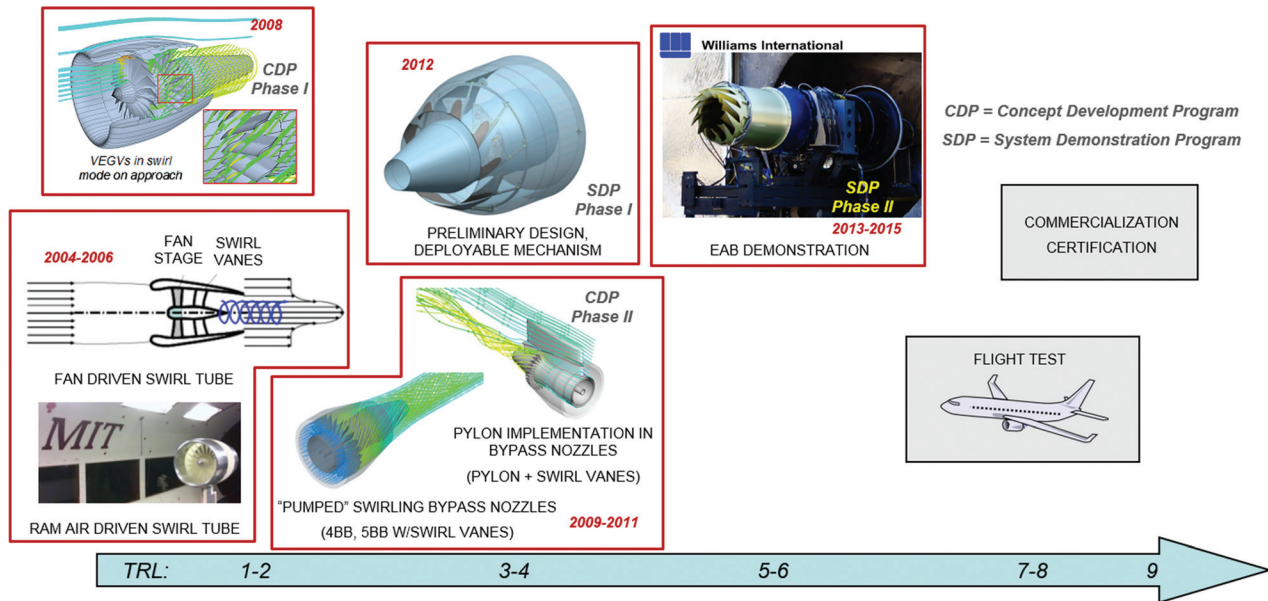
Fig. 1 Technology development roadmap in context of NASA TRL definitions

PC-24 and is a medium-bypass, twin-spool design with four compression stages and three turbine stages that produces 3621 lb (16.11 kN) of takeoff thrust at sea level static conditions, flat-rated up to 79 °F (26 °C). The current paper presents the outcomes of the culmination of the system demonstration program, in which the EAB mechanism was demonstrated on a full-scale operating FJ44-4 A.

Technical Objectives

The technical objectives were as follows:

(1) Design, fabricate, and test a realistic flight-weight EAB on a modern turbofan propulsion system.
(2) Quantify the equivalent drag, effect on operability, and noise of such a system.
(3) Perform system-level analysis of the proposed impact in terms of steep descent for noise reduction and other applications.

The demonstration goal for the mechanical prototype was to seamlessly switch between stowed and deployed modes (see Fig. 2) while the engine operated at its highest thrust setting for an approach scenario, called dirty approach. This condition represents a scenario where the airplane is in an aerodynamically unclean configuration, with high-lift and high-drag devices
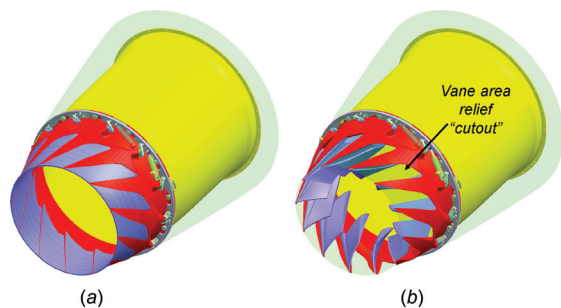

Fig. 2 EAB CAD model in two configurations. Translucent green region shows allowable zone boundary. Vane area cutout feature controls effective exit area: (*a*) stowed and (*b*) fully deployed (100 deg).

deployed, and the engine operates at a relatively high power setting to meet go-around spool-up time and hot bleed air requirements for the aircraft anti-icing system.

Design Requirements (Success Goals)

Design requirements were established by ATA, WI, and NASA to ensure a safe and successful ground testing campaign and to demonstrate that the EAB could be integrated into a typical aircraft installation such as the Cessna CJ4.

Aerodynamic requirements:

(1) no measureable thrust or thrust-specific fuel consumption penalty in the stowed configuration,
(2) a 15% net thrust reduction at dirty approach fan speed ($N1$) in the fully deployed configuration, measured as a percentage of the stowed nozzle's gross thrust at the same condition,
(3) no measurable fuel consumption penalty when fully deployed,
(4) no measurable flow reduction when deployed, and
(5) adequate surge margin during all operation, including dynamic deployment and stowing.

Structural requirements:

(1) acceptable static strength factors of safety,
(2) acceptable high-cycle fatigue life on parts,
(3) acceptable response to expected sine and broadband excitation sources, and
(4) adequate thermal margin for selected materials.

Mechanical design constraints:

(1) demonstration of dynamic deployment in 3–5 s,
(2) demonstration of dynamic stowing in <0.5 s, to ensure that the EAB does not interfere with thrust recovery in a go-around event, and
(3) packaging of the EAB nozzle and its deployment mechanism within a notional aircraft cowl.

The packaging requirement was addressed by defining an axisymmetric allowable zone (shown in Fig. 2) based on an equivalent average diameter of a typical (nonaxisymmetric) flight cowl. The entire EAB mechanism had to be contained within this zone to meet the design requirement. In addition to these ground testing requirements, additional flightworthiness requirements that were considered included (1) a desired maximum weight, (2) the ability
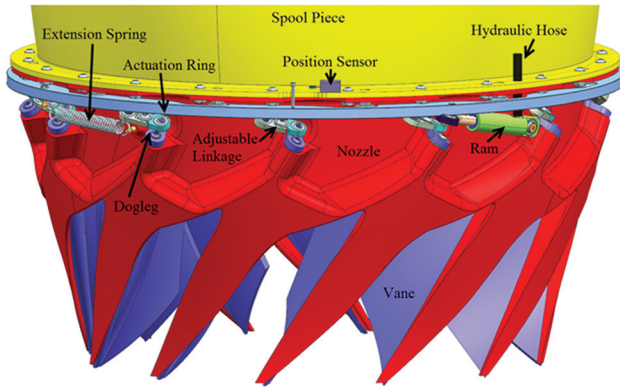
Fig. 3 Key components of the EAB assembly

Fig. 4 Photographs of the assembled EAB nozzle: trimetric view (left) and aft-looking-forward view (right)

to integrate the EAB with aircraft hydraulics, and a (3) a minimal noise penalty, including no spurious tones associated with modifications to the exhaust geometry in the deployed state. Since the planned tests were primarily for performance demonstrations, it was assumed that noise deltas would be sufficient to measure on the test stand.

Mechanical Design

The EAB assembly consists of the following main components, pictured in Fig. 3: a spool piece, an aluminum nozzle, 12 high-temperature aluminum vanes, 12 stainless steel shafts (not pictured), 12 dogleg lever arms, 12 adjustable linkages, three hydraulic rams, three extension springs, a stainless steel actuation ring, and a string potentiometer for ring position sensing.

The nozzle was designed with cutout cavities on its inner surface to house the vanes. This allows the nozzle plus vanes to have the same inner mold line as the baseline nozzle when the vanes are in the stowed position. The nozzle and vanes were designed to create an effective lap seal when in the stowed position, with dimensions toleranced to minimize any performance loss from gaps between the mating parts. The nozzle's outer surface matches that of the allowable zone starting at the trailing edge and moving upstream until the bearing blocks, where it drops to a reduced diameter to allow space for the bearing blocks and mechanisms. The nozzle bearing blocks house two press-fit bushings that support each shaft. This allows each shaft to rotate freely to deploy each vane.

A key design feature of the EAB is that a significant fraction of the suction side of the vane is actually exposed to the external flow when stowed—i.e., the vane contains a surface that would normally be defined by the aircraft engine external cowl in a conventional configuration. In this way, when the vanes deploy, they actually open up a "cutout" region (see Fig. 2), allowing the nozzle to regulate the effective $A8$ of the nozzle and thereby mitigate or even reverse loss of surge margin relative to the conventional "round" nozzle operation.

The rotation of the shaft and vanes is driven by the actuation ring. It is mounted on V-groove bearings that thread into the nozzle flange. The ring rotates when a load is applied to it by the three hydraulic rams. These rams are mounted to the nozzle via spherical bearings and steel inserts. The rams can provide up to 600 lb force each when operated at 3000 psi.

When the actuation ring rotates, it pulls on the adjustable linkages connected to the dogleg lever arms of each shaft, causing each shaft and vane to rotate. The adjustable linkages are connected to the dogleg and ring using spherical bearings and shoulder screws. This allows the system to accommodate the tilted axes of the shafts, which are aligned with the swirl angle of the EAB, without interfering with the free motion of the spherical bearings. The clocking of the linkages is designed such that the angle of their lever arm with the dogleg is optimal for deploying

the vanes out of the initial stowed position and holding them in the maximum deployed position where aerodynamic loads are highest.

The assembly also contains three extension springs mounted to the nozzle in a fashion similar to the hydraulic rams. These extension springs have an initial preload to ensure that the vanes remain in the stowed position when hydraulic pressure is released.

The ring position sensor is a string potentiometer connected to the downstream flange of the spool piece. The eyelet of the string potentiometer connects to a pin on the actuation ring such that it will extend the string of the string potentiometer when the actuation ring rotates.

Photographs of the assembled EAB nozzle are shown in Fig. 4.

Aerodynamic Design

The aerodynamic design space was investigated with a computer-aided design (CAD) parametric model of the nozzle and deployable vanes. EAB vane geometries were studied for a number of parameters, including vane count, swirl angle, full deployment rotation angle, chord length, area relief depth, and leading-edge sweep angle.

Computer-aided design models were converted into circumferentially periodic computational fluid dynamics (CFD) fluid domains to predict aerodynamic performance. To cope with the nonuniformity of flow emanating from the 14-lobe mixer, a mixing-plane interface was introduced to study the loading from arbitrary vane counts. While the mixing plane circumferentially averaged out some of the nonuniformity associated with the mixed flow, it was an efficient approach to exploring the design space.

A typical CFD domain is pictured in Fig. 5. Steady Reynolds-averaged Navier–Stokes CFD simulations were performed using an ideal gas air model with coupled flow and energy equations. The k–ω shear stress transport (Menter) turbulence model was selected with an "all y^+ wall treatment," which automatically resolves the viscous boundary layer if the wall-normal cell size is adequately fine and smoothly switches to a wall-function model if
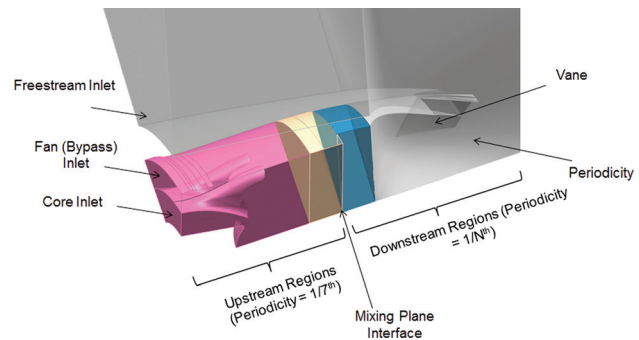

Fig. 5 Zoomed-in view of typical CFD domain for arbitrary vane count used a mixing-plane interface
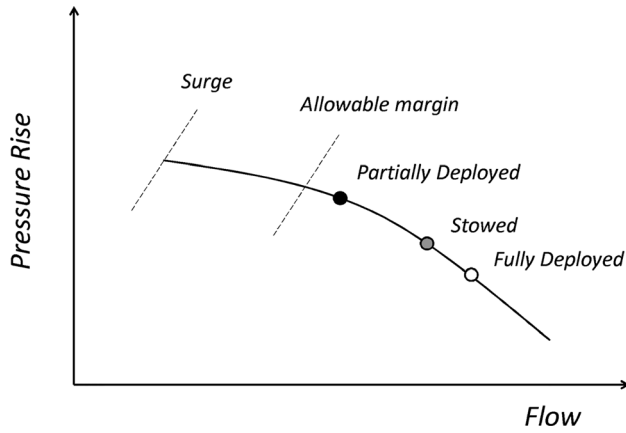
Fig. 6 Conceptual depiction of engine fan operating point for EAB in different configurations

it is not. Typical mesh sizes for these circumferentially periodic domains were $3–5 \times 10^6$ cells for the final designs. Select full-annulus simulations were eventually performed on the final designs to verify consistency with the partial circumferential sector models.

At arbitrary deployment angles between stowed and fully deployed, the effective flow capacity of EAB nozzle varies, and the engine responds by rematching at fixed *N1*. During deployment, a reduction of flow capacity is experienced at partial angles before an overall increase in flow capacity is experienced in the fully deployed state. This is due to the competing effects of (1) swirl and drag monotonically increasing with deployment angle, which reduces flow capacity, and (2) the degree to which the

(a)

(b)
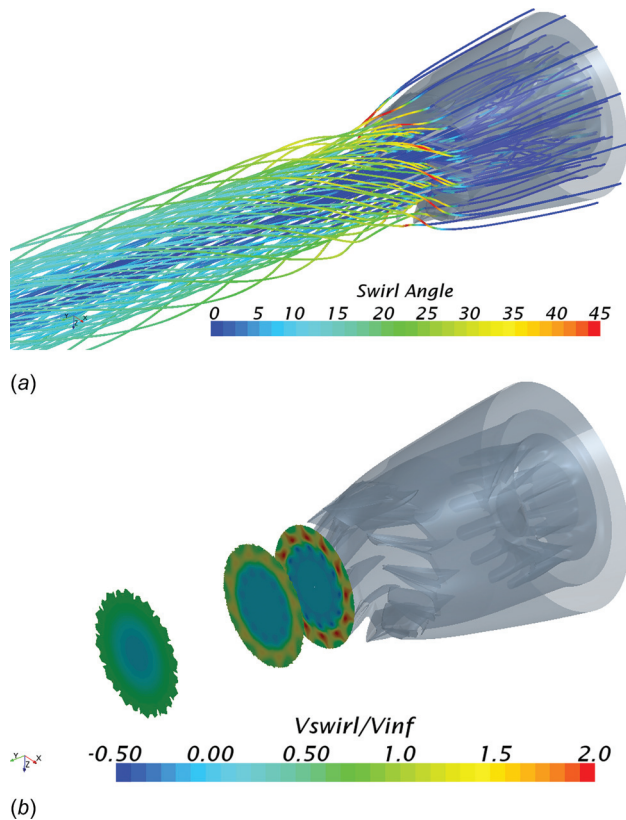
Fig. 7 Mixing-plane CFD results for final design in fully deployed (100 deg) configuration: (a) circumferential (swirl)-to-freestream velocity ratio, selected downstream exhaust planes and (b) streamlines colored by swirl angle

Table 2 Key aerodynamic features of final design

Parameter	Value
Vane count	12
Vane swirl angle	34 deg
Vane full deployment rotation angle	100 deg
Leading-edge sweep angle	35 deg
Vane area relief cutout depth (percent of local chord)	70%

deployment angle exposes the cutout region (pictured in Fig. 2), which increases flow capacity. This is illustrated conceptually in Fig. 6. To set the appropriate boundary condition for the EAB at fixed *N1*, a fan rematching model was implemented as a macro in the CFD solver to adjust the fan and core inlet boundary conditions to comply with the engine's pumping characteristics.

Contours of dimensionless swirl velocity (normalized to the approach flight velocity) and streamline patterns from the stowed and fully deployed final design are shown in Fig. 7. The swirl velocity contours suggest that the flow becomes axisymmetric about two nozzle diameters downstream of the vanes. The streamlines are colored by swirl angle, defined as the arctangent of the ratio of circumferential to axial flow velocity. Locally in the vane passages the swirl angle is 30–35 deg, consistent with the design of the vanes. Key features of the final aerodynamic design are given in Table 2.

Full-Scale Engine Testing

The primary engine testing objectives were to measure the performance of the stowed and deployed EAB to quantify the equivalent drag via thrust reduction, the effective flow capacity (to assess the impact of the EAB on operability), and the change in near- and far-field noise, and to demonstrate controlled deployment and stowing on time scales set in the design requirements specification. Secondary objectives were to measure mean and
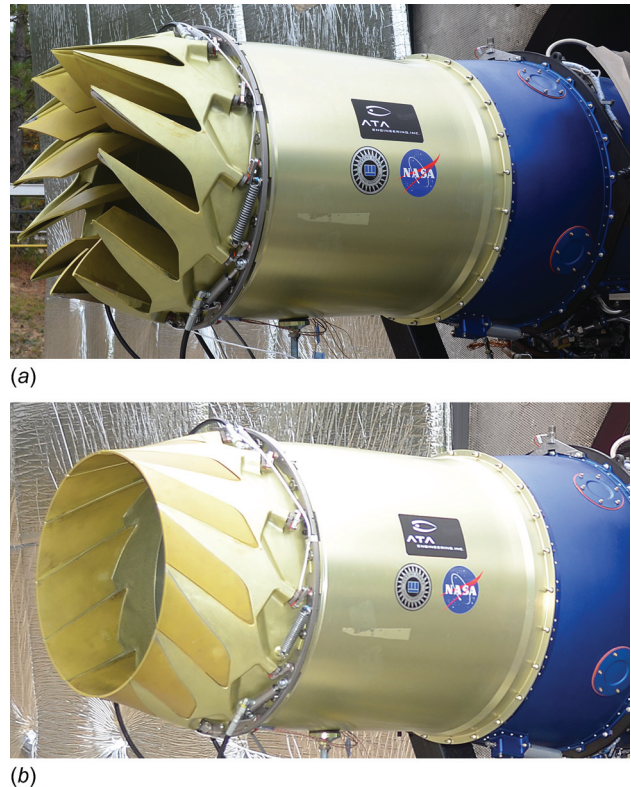

(a)

(b)

Fig. 8 Two EAB nozzle configurations on FJ44-4 engine: (a) EAB fully deployed and (b) EAB stowed
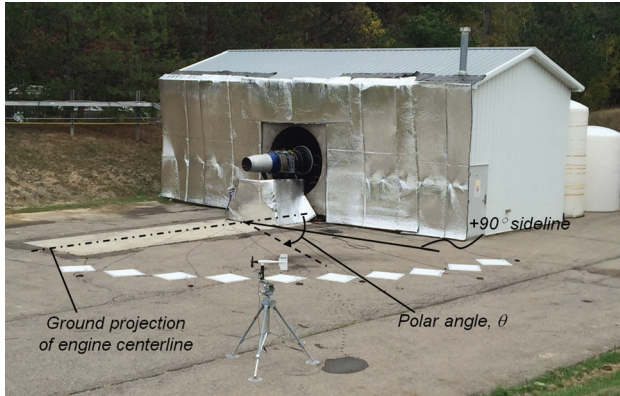
Fig. 9 View of engine on OTF2 test stand with far-field microphone on white ground plates arranged in a polar arc array (90–162 deg). Anemometry station in foreground.

fluctuating stresses on the vane to assess structural design margins and estimate life from cyclic pressure and thermal loading. The test plan was structured to address all technical objectives in a manner that allowed an incremental approach to risk reduction.

Three key nozzle configurations tested were the fully deployed EAB, the stowed EAB, and the WI referee nozzle. The two EAB configurations are pictured in Fig. 8, and the referee nozzle is pictured from a distance in Fig. 9. The inner flowpaths of the stowed EAB and the WI referee nozzle were identical. In addition to the configurations pictured, partially deployed angles were tested using position locks to hold the deployment angle fixed.

The EAB nozzle assembly was instrumented by ATA to monitor its performance; instrumentation included strain gages, thermocouples, and accelerometers. Additionally, a string potentiometer signal was used to monitor the deployment angle of the EAB vanes. The FJ44-4 A engine and test facility were instrumented by WI to measure engine and test facility performance parameters (e.g., thrust, airflow, fuel flow, pressures, temperatures, shaft speeds, vibration, and environmental conditions). Far-field noise was measured at ten positions on a polar array of microphones located on the ground, radially twenty nozzle diameters from the nozzle exit plane, as shown in Fig. 9.

The facility used for the test program was outdoor test facility #2 (OTF2) at WI's complex in Walled Lake, MI. This facility is used for testing jet engines of up to 6000 lb thrust. The 6000 lb thrust capacity thrust stand has a 6×2.5 ft thrust bed and is protected by a roofed structure with roll-up doors on all four sides. A 10×20 ft portable control room located about 150 ft away houses a control console, automatic controls, recorders, and computer equipment.

Performance and Operability

The success goals for the aerodynamic performance and operability of the EAB were to meet the criteria specified in the design requirements section, particularly the 15% thrust reduction in the fully deployed configuration.

The stowed EAB nozzle was tested up to 100% corrected fan speed in two configurations: an as-built configuration and a configuration with gaps (see mechanical design section) taped to inhibit leakage flow. Upon completion of the testing, the WI performance and operability team analyzed the data and determined the following:

(1) Comparison of the stowed EAB nozzle to the WI referee nozzle indicated that the thrust was lower by about 1%.
(2) There was no appreciable performance difference between the two configurations, suggesting that leakage through the lap seals formed between EAB vanes and the fingered nozzle was minimal.
(3) Comparison between the initial and final performance calibrations with the WI referee nozzle suggested that engine performance did not change over the course of the testing.
(4) The initial and final performance calibrations with the EAB nozzle also matched, suggesting that the EAB device did not change during testing.
(5) The EAB nozzle, when stowed, appeared to behave slightly more open in $A8$ than the WI referee nozzle. The trends in thrust, interturbine temperature, airflow, fuel flow, high-spool speed $N2$, and fan tip pressure ratio were all reasonably simulated with a small $A8$ increase.
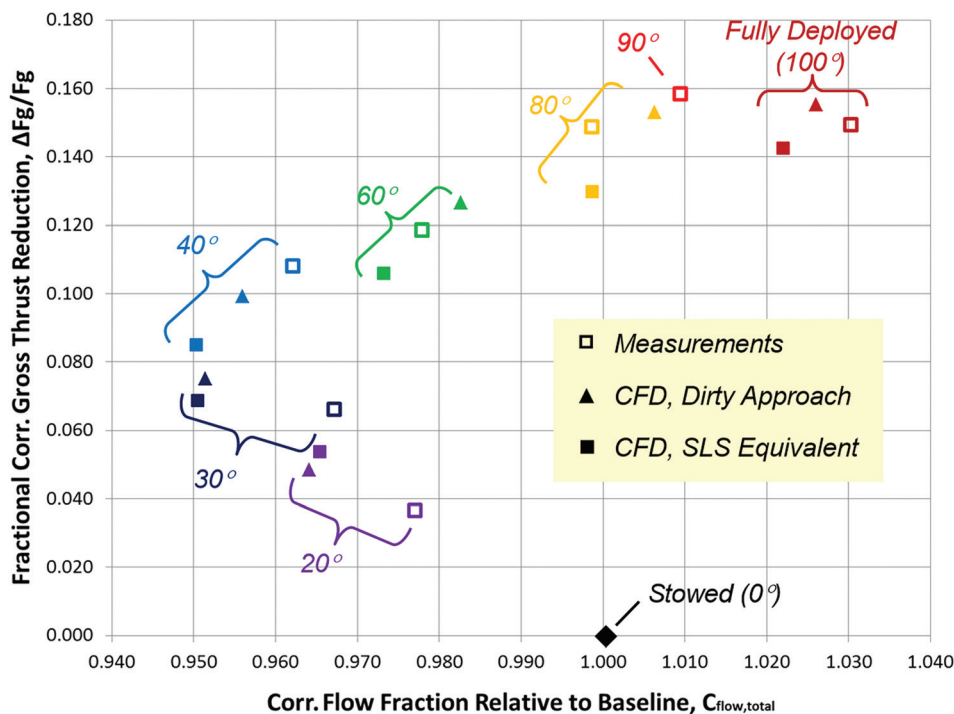
Fig. 10 $\Delta F_g/F_g$ versus fractional flow capacity for EAB at various deployment angles
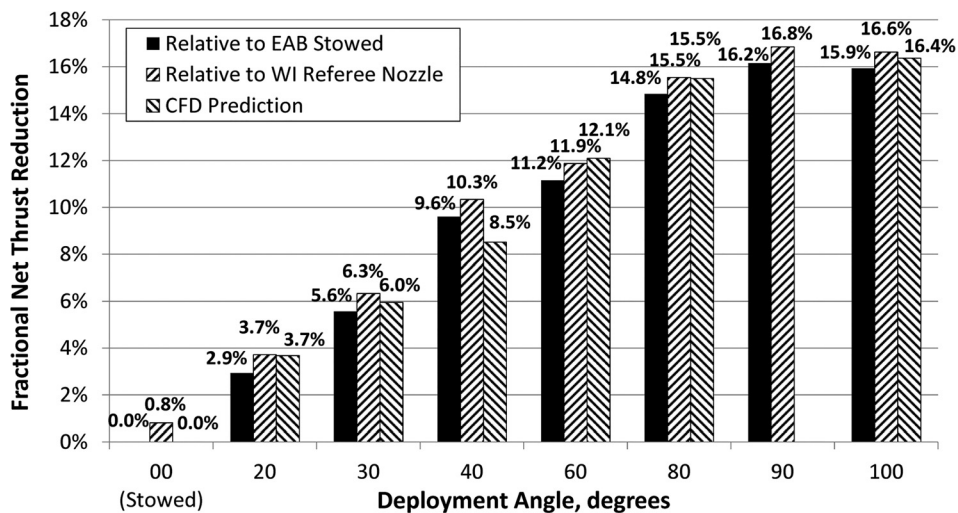
Fig. 11 Measured net thrust reduction ($\Delta F_n/F_g$) from stowed (0 deg) to fully deployed (100 deg)
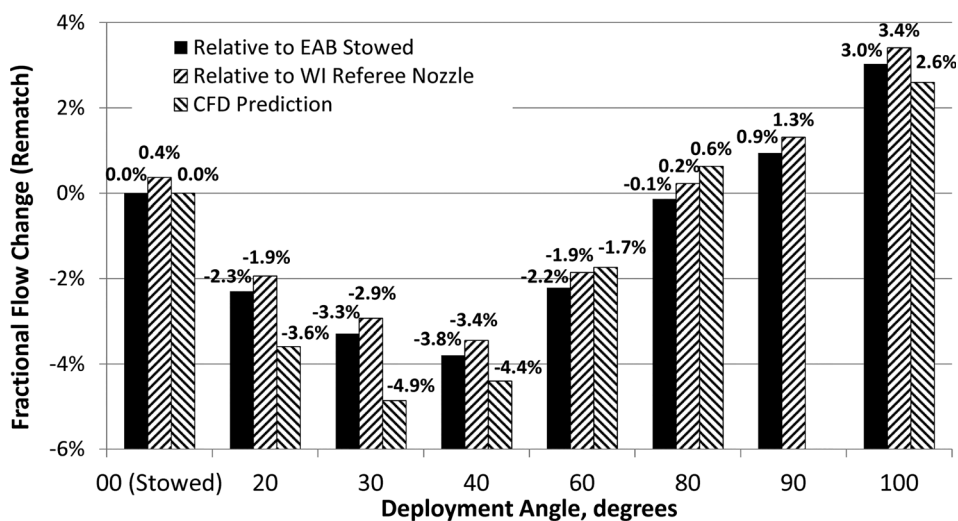

Fig. 12 Measured fractional flow change (rematched) from stowed (0 deg) to fully deployed (100 deg)
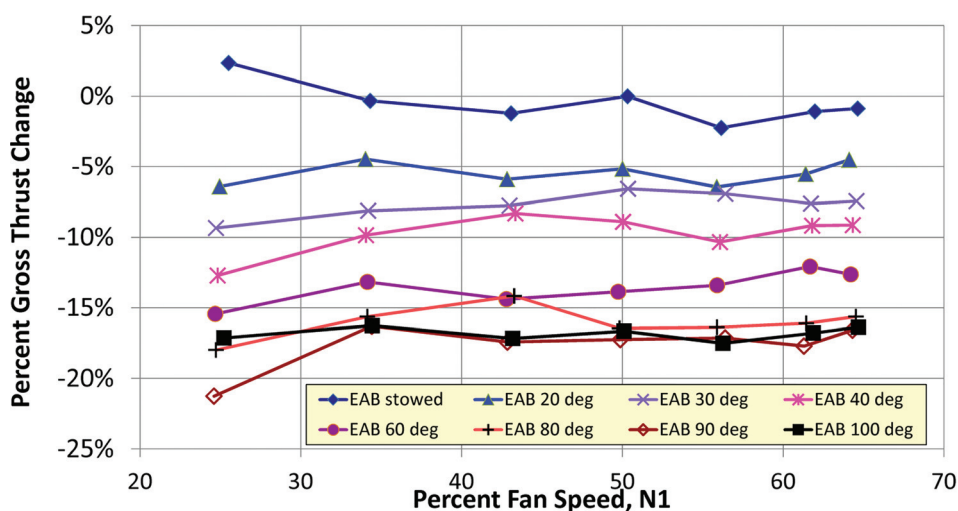

Fig. 13 Percent gross thrust change versus percent fan speed ($N1$) EAB at various deployment angles
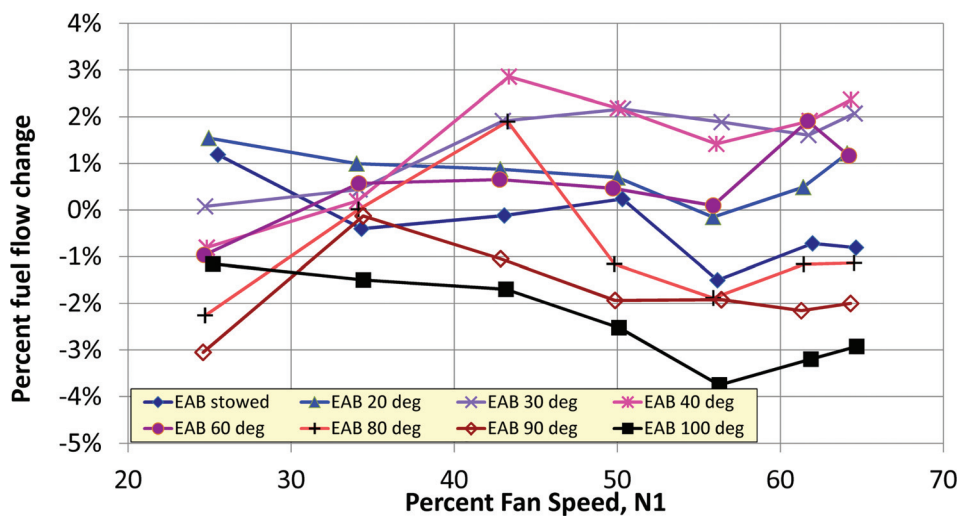
Fig. 14 Percent fuel flow change versus percent fan speed (*N*1) EAB at various deployment angles
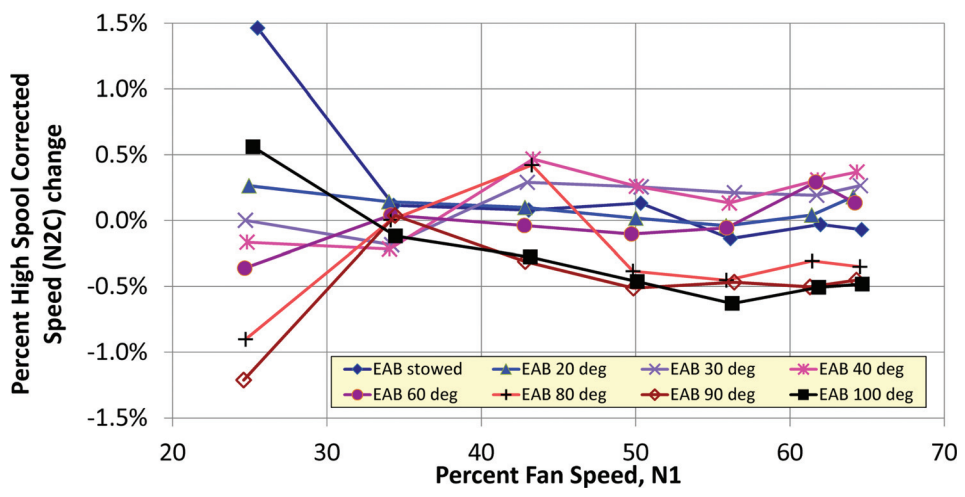

Fig. 15 Percent corrected *N*2 speed (*N*2*C*) versus percent fan speed (*N*1) EAB at various deployment angles
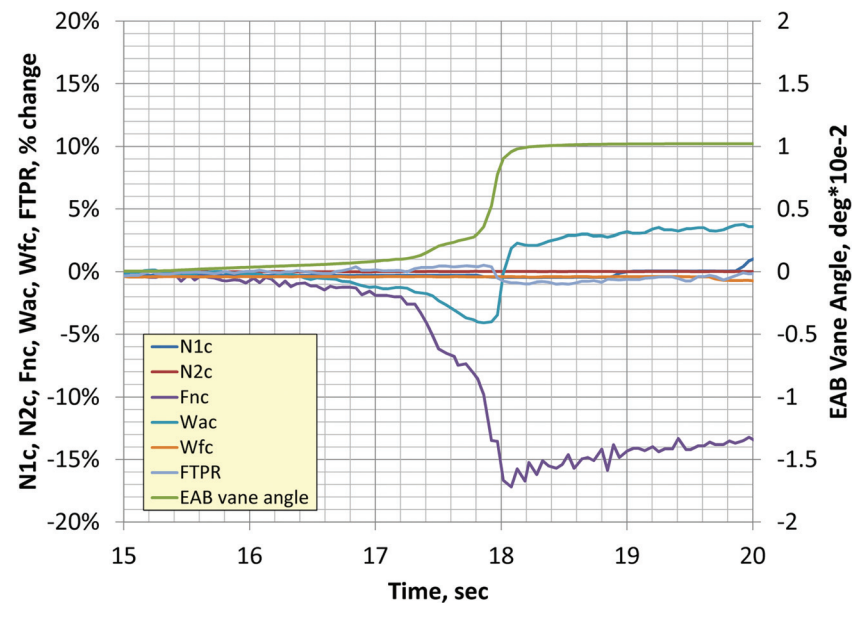

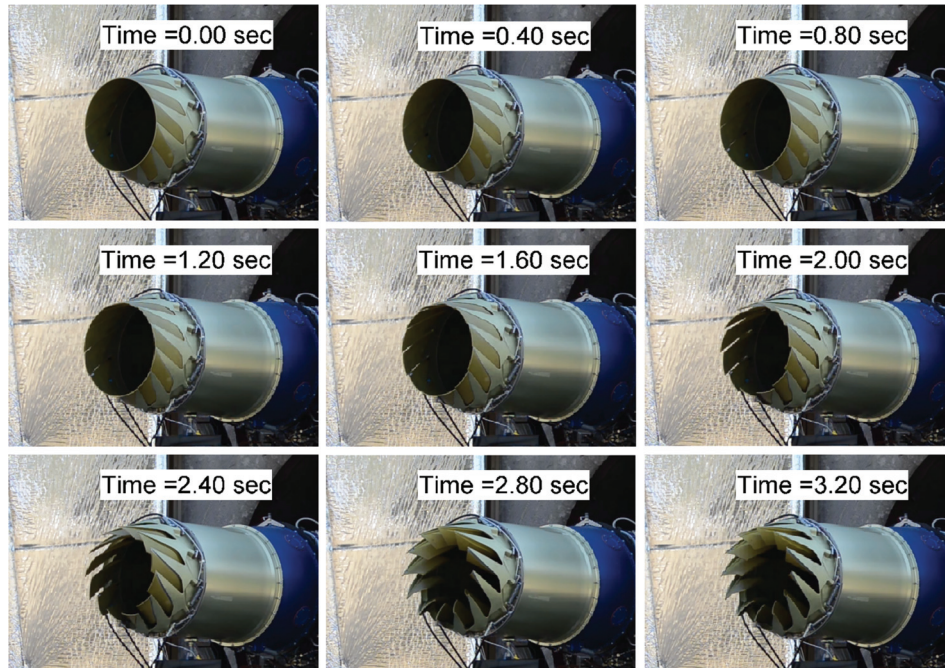**Fig. 16** Transient data during deployment

Fig. 17 Frame-by-frame video analysis of deployment, showing 3–5 s duration
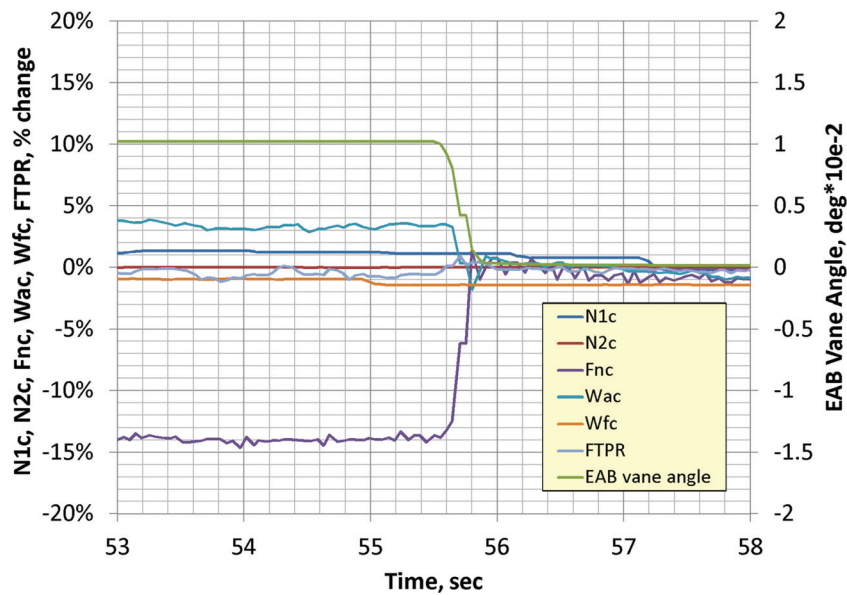

Fig. 18 Transient data during stowing

Based on this analysis, the conclusion was that the stowed EAB did not introduce any performance deterioration that is fundamental to its design. It would be straightforward to introduce very minor dimensional changes to a follow-on design to further optimize the exhaust nozzle nominal area when in operation. The increase in nozzle flow coefficient is estimated to correspond to the radial opening of the nozzle, which occurs under pressure loads when in operation (i.e., the EAB nozzle did not have the "hoop strength" of the round referee nozzle).

Given the small $A8$ difference between the EAB stowed nozzle configuration and the WI referee nozzle, it is worth noting that performance deltas for thrust reduction and flow capacity change could be presented using either nozzle as the baseline. In terms of the EAB design requirements, it was determined that the stowed EAB configuration would be the more appropriate (and

conservative) choice to assess both thrust reduction and flow capacity change, since the deltas would be measured for the same device in two of its configurations.

Figure 10 gives the fractional gross thrust reduction as a function of flow fraction for each of the partially deployed EAB configurations. Open squares represent measured data, closed squares represent CFD results performed in ground conditions (near sea-level static external flow), and closed triangles represent the same CFD predictions assuming the dirty approach external flow Mach number of about 0.2. Qualitatively, the measured data follow the trends predicted by the CFD, with the worst flow capacity occurring between 30 deg and 40 deg deployment. As noted earlier, the initial reduction in flow capacity occurs because the partially deployed swirl vanes are seen as a blockage in the nozzle, while the fully deployed vanes have exposed the area relief feature
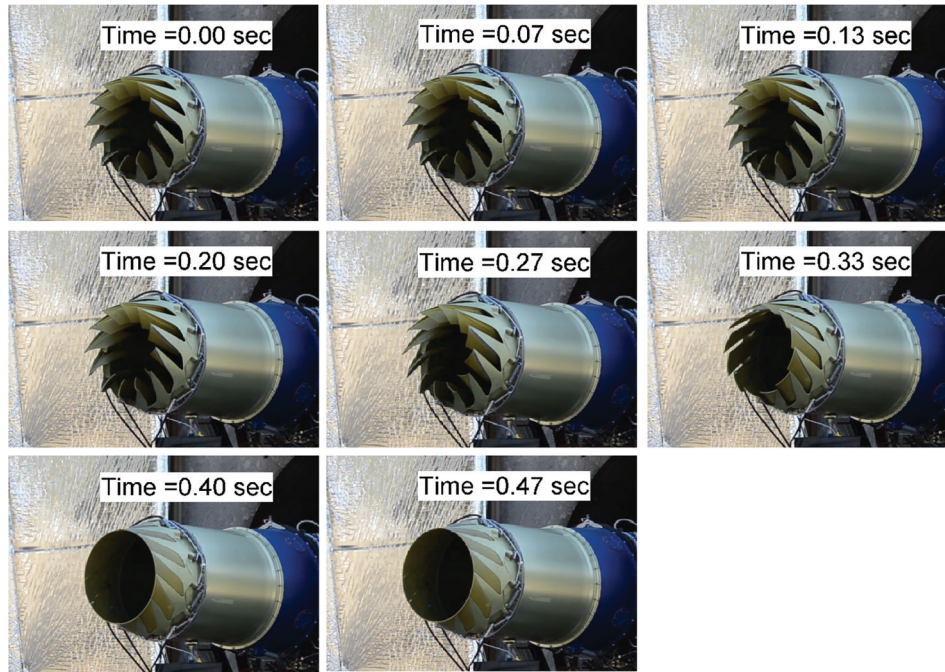
Fig. 19 Frame-by-frame video analysis of stowing, showing < 0.5 s duration

referred to as the cutout. Quantitatively, the fractional gross thrust reduction (as a fraction of nominal gross thrust) is only slightly higher in the measured data than in the CFD predictions. At the fully deployed state, the fractional gross thrust reduction is 15.0%, and the rematched flow capacity increase is 3.0%. When accounting for the additional ram drag given by the increased flow in an approach scenario at about 120 kn (see Table 1), the deployed EAB achieves 15.9% net thrust reduction (as a fraction of nominal gross thrust), exceeding its 15% target.

Figure 11 presents the measured and predicted net thrust reduction fraction (normalized to baseline gross thrust) as a function of deployment angle. Using either the stowed EAB nozzle or the WI referee nozzle, the predictions were consistent with the measurements to within about 1% of gross thrust at all angles except 60 deg, where the predictions agreed to within 2%. In terms of the target thrust reduction of 15% of gross thrust, the predictions were within 13% (i.e., 2/15).

Figure 12 presents the measured and predicted rematched flow fractions (normalized to baseline corrected flow) as functions of deployment angle. Relative to either the stowed EAB nozzle or the WI referee nozzle, CFD predictions were consistent with the measurements to within about 1% of gross thrust at all angles except 20 deg and 30 deg, and their deviations were always in the favorable direction in terms of operability.

Figures 13–15 present the percent gross thrust change, percent fuel flow change, and percent high-pressure spool corrected speed change as functions of fan speed for each EAB configuration. These percent changes are relative to the WI referee nozzle. The range of tested fan speeds spans the ground idle ($\sim$25%) to dirty approach ($\sim$65%) throttle settings. The dirty approach design condition was thus well above flight idle ($\sim$33% $N1$), which was the second-to-lowest throttle setting.

In terms of gross thrust change, the EAB's performance at different deployment angles is generally consistent across the range
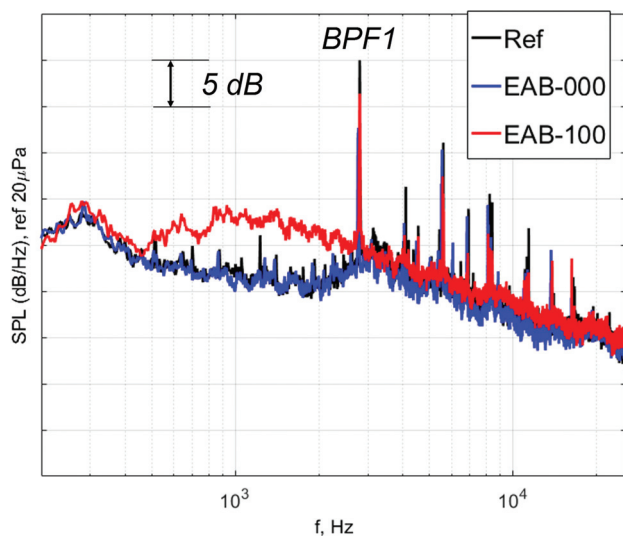

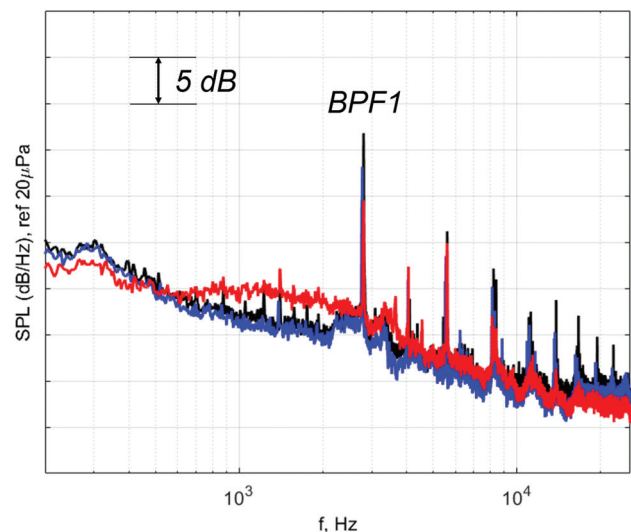**Fig. 20 Narrowband (4 Hz) SPL spectra at polar angle $\theta = 90$ deg**

Fig. 21 Narrowband (4 Hz) SPL spectra at polar angle $\theta = 130$ deg. Ordinate values arbitrarily shifted relative to previous figure to conceal absolute levels.
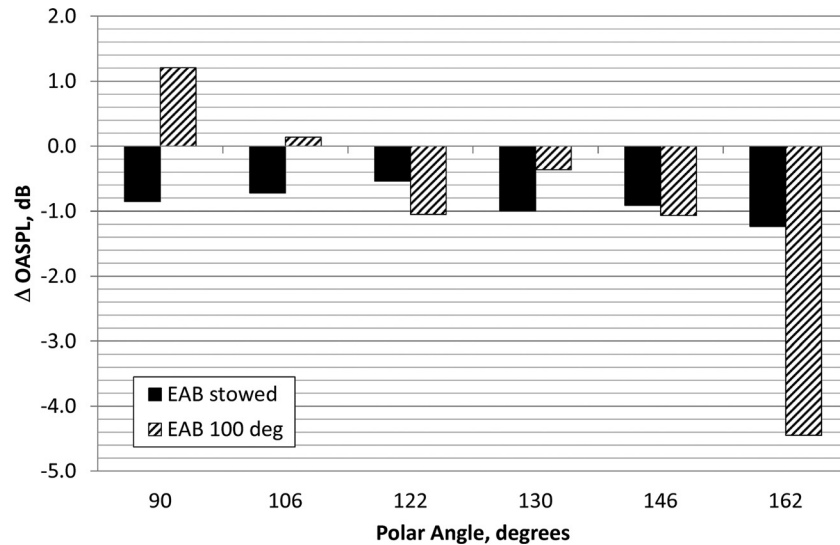
Fig. 22 OASPL deltas relative to referee nozzle at dirty approach power condition at six polar angles. Negative ordinate values indicate noise reduction.

of speeds. The fuel flow fraction is seen to decrease by about 3% in the fully deployed configuration at dirty approach, a consequence of engine rematching to a larger effective $A8$. This reduction in fuel flow appears consistent with a reduction in high-pressure spool corrected speed ($N2C$) and indicates that the deployed EAB may also be useful for reducing overall fuel consumption during descent and approach, both by shortening the time to descend and by reducing the fuel burn during descent.

Dynamic Stowing and Deployment

Dynamic deployment and stowing were achieved using the EAB hydraulically actuated rams. The hydraulic pump and needle valves were operated remotely (from the control room) to command the EAB to the deployed or stowed position.

Figure 16 plots transient data recorded during the dynamic deployment that satisfied the 3–5 s requirement. Shown on the plot are time histories of percent changes for both corrected speeds ($N1C$ and $N2C$), corrected thrust (Fnc), corrected air flow (Wac), corrected fuel flow (Wfc), and fan tip pressure ratio, in addition to vane deployment angle as measured by the string potentiometer. The time on the ordinate is measured from the beginning of data recording. Figure 17 shows frame-by-frame video analysis of the corresponding event (using a shifted time- = 0 s marker selected arbitrarily close to the beginning of the deployment event). The time history of the recorded signals shows that the vanes deploy in about 3.5 s, with the thrust reduction occurring in correspondingly similar time. The flow capacity of the now slightly more open nozzle is also adjusted in the same time scale. Lagging behind this is the inertia of the rotor, which for a fixed throttle angle setting adjusts itself about 1% higher. As can be seen from the plot, the thrust reduction is between 13% and 14% but would satisfy the 15% target if the full-authority digital engine control were programed to hold $N1C$. During dynamic testing, several runs were performed where the $N1C$ value was adjusted back to the nominal value after the transient associated with dynamic deployment had stabilized. When this was done, the 3% fuel burn benefit was realized.

Figure 18 shows the same recorded data during the stow event. This figure is part of the same data run as the previous one, and it can be seen that the $N1C$ value was still high by ∼1% when the vanes were stowed, thereby returning the system to the original thrust and speed. Stowing occurred in about 0.3 s, greatly assisted by the aerodynamic loading on the vanes, as seen in Fig. 19.

Far-Field Acoustics

Narrowband (4 Hz) sound pressure level (SPL) spectra at polar angles $\theta = 90$ deg and 130 deg are shown in Figs. 20 and 21 for the WI referee nozzle (black, "Ref"), the stowed EAB (blue, "EAB-000"), and the deployed EAB nozzle (red, "EAB-100") at the dirty approach power condition. The spectra show a combination of broadband noise dominated by the jet source, superposed with shaft harmonic tones. The most prominent tone at the fan rotor first blade-pass frequency occurs at 16 times the $N1$ shaft speed angular frequency. In general, the deployed EAB shows a broadband jet mixing signature that is characteristic of a mixing enhancement device, with midfrequency noise increase at the side directivity angles (e.g., 90 deg), and low-frequency noise suppression at the aft directivity angles (e.g., 130 deg).

Interestingly, the strength of the fan first blade-pass tone showed some suppression with both the stowed and deployed EAB nozzle relative to the referee nozzle. The change in the integrated metric overall SPL (OASPL) is given in Fig. 22. In this plot, it is seen that the tone noise suppression actually lowers these noise metrics at many of the emission angles. Additionally, the EAB in its deployed configuration is generally within 1 dB relative to the stowed configuration at most of these angles. This is a favorable finding, suggesting that after accounting for the effect of forward flight (which tends to suppress swirling jet noise less effectively than straight jet noise [21]), the system-level effect of the EAB on perceived noise will allow an aircraft to take advantage of the steep approach noise suppression effect associated with moving the sound sources farther away from the airport community.

System-Level Implications

The constant-speed approach scenario discussed in the introduction was applied to the Cessna CJ4 at a maximum landing weight of 15,500 lbf. The conventional 3 deg glideslope was compared to the steeper glideslope of 4.3 deg enabled by the EAB's equivalent drag due to thrust reduction. It is worth reiterating that since the maneuver is simulated at constant speed, the aerodynamics of the airframe, including its lift, drag, and noise, remain unchanged;[4] the

---

[4]This assumption of unchanged vehicle aerodynamics is strongest for aft-fuselage engine installations. In an under-wing installation, some interaction may be anticipated between the swirling exhaust and the wing in a high-lift configuration, and this warrants further study. However, the streamtube boundaries of the swirling flow exhausting the nozzle are not expected to be altered drastically (e.g., see Fig. 7).

Table 3 ANOPP study summary for a constant V_{app} dirty approach scenario. Glideslope increase in second column is based on a 3 deg baseline approach.

Jet noise impact	Gross thrust reduction (%)	$\Delta\Theta \sim \Delta$ $(\Delta\text{-}T)/\Omega$(deg)	ΔEPNL (dB)	ΔPNLT max (dB)	ΔPNLT initial (up range) (dB)
Jet noise penalty $+9.3$ dB (inclusive of swirling flow and flight effect)	15	$+1.3$	-1.1	-2.2	-7.9
Measured static ΔSPL, all angles, no flight effect	15	$+1.3$	-3.1	-4.5	-11.3
Measured static ΔSPL, all angles, $+2.5$ dB flight effect penalty	15	$+1.3$	-2.8	-4.3	-10.7

difference in perceived noise is due to the steeper glideslope coupled to any increase in jet noise associated with the swirling exhaust. In terms of $C_{d,\text{eq}}$, the demonstrated 15% thrust reduction is equivalent to about one bluff-body having the cross-sectional area of the sum of two engine fan faces.

Table 3 presents the results of an aircraft noise prediction program (ANOPP) comparison study between the two approach trajectories under various assumptions for jet noise penalty. Ahead of the present engine testing, a more severe 9.3 dB jet noise penalty was estimated using previously measured noise data on separate flow nozzles [20,21] that included the effect of forward flight. Under this scenario, the EPNL metric still showed a 1.1 dB noise benefit. An alternative scenario using only measured static noise deltas at all polar angles to capture the directivity (without the effect of forward flight) suggests a 3.1 EPNdB noise reduction. A more realistic forward flight effect penalty, based on the separate flow nozzle data and the measured gross thrust reduction, would be about $+2.5$ dB based on static-to-flight deltas measured in previous nozzle tests [21]. The resulting noise reduction is 2.8 EPNdB. In all cases, the benefit of the EAB is seen and may be combined with several of the other measured benefits of the device such as fuel burn reduction on descent and approach, plus access to steeper approaches, to improve system performance.

Conclusions

Full-scale ground engine testing of the EAB on the FJ44-4 A verified the following:

(1) The EAB met its fully deployed equivalent drag target of at least 15% thrust reduction at constant fan speed for the dirty approach power condition.
(2) All nozzle flow capacity targets were met across the range of stowed to fully deployed rotation angles. It was demonstrated that the EAB did not compromise engine operability during dynamic deployment or stowing.
(3) The broadband noise increase from the swirling jet exhaust flow was modest, which allows the EAB to enable system-level steep approach scenarios that provide system-level noise reduction.
(4) Dynamic deployment was demonstrated in 3–5 s and stowing was demonstrated in less than 0.5 s—fast enough to support go-around requirements.
(5) EAB thermal environments were within predicted limits, and structural dynamic environments were benign.
(6) Differences in the performance between the stowed EAB and the WI referee nozzle of equal (cold) design $A8$ could be attributed to effective area change, suggesting that the EAB could be designed to match round nozzle performance in the stowed configuration, thereby avoiding cruise performance penalties.
(7) The larger $A8$ in the fully deployed configuration resulted in a beneficial rematch of the $N2$ spool, leading to about 3% fuel burn reduction, which could be combined with faster descent rate to reduce overall fuel burn; fuel weight savings may potentially be used to mitigate the EAB's weight penalties to help it buy its way onto an aircraft.

The ultimate conclusion from the technical effort was the advancement of the TRL of the EAB from 3–4 at the onset of the program to six at its completion. The EAB testing demonstrates an unconventional benefit derived from an engine technology in order to reduce the impact of airframe noise. Additionally, it will enable greater access to confined airports, more rapid descent resulting in fuel burn reduction (which may offset any additional weight required by the devices mechanism), greater access to CDAs, and reduction of thrust in icing conditions when hot bleed air is required by the aircraft's anti-icing systems. These benefits are expected to be applicable to business jets, large commercial aircraft, and military transports.

Outlook

Flight testing is a next logical milestone that must be achieved to bring TRL to seven and beyond. Toward this end, several future work steps are recommended:

(1) Light weighting of the nozzle assembly; the present design uses solid aluminum vanes, for example, whose weight could be significantly reduced through material or design changes.
(2) Demonstration of minimum durability and reliability, e.g., ground testing on the engine that includes cycling (deployed/stowed) of the EAB with steady-state operation through a typical mission profile for a specified number of hours.
(3) Integration into an experimental aircraft, e.g., a modified aft cowl with bleed slots and new loft lines, routing of accessories, improved reliability of hydraulic/control system, flight deck control (on/off switch), and assessment of the forces imparted by the EAB that must be reacted by the aircraft control surfaces.
(4) Flight test planning, e.g., typical takeoff/climb profiles during stowed EAB configuration, descent and approach profiles with deployed EAB configuration.
(5) Design modifications for high-power deployment up to 10 deg for potential jet noise reduction from subtle shear-layer modification.

Nomenclature

$A8$ = nozzle exit area
ANOPP = (NASA's) aircraft noise prediction program
A_{ref} = reference area

$C_{d,\mathrm{eq}}$ = equivalent drag coefficient
D = drag
F = thrust
F_g = gross thrust
F_n = net thrust
Fnc = net corrected thrust
M_∞ = Mach number
$N1$ = fan rotational speed
$N1C$ = fan corrected rotational speed
$N2C$ = high-spool corrected rotational speed
OASPL = overall SPL
SPL = sound pressure level
$V_{\mathrm{app.}}$ = approach velocity
W = aircraft weight
Wac = corrected air flow rate
Wfc = corrected fuel flow rate
θ = glideslope angle
ρ_∞ = freestream density

References

[1] Manneville, A., Pilczer, D., and Spakovszky, Z. S., 2006, "Preliminary Evaluation of Noise Reduction Approaches for a Functionally Silent Aircraft," J. Aircr., 43(3), pp. 836–840.

[2] Hileman, J., Reynolds, T., de la Rosa Blanco, E., Law, T., and Thomas, S., 2007, "Development of Approach Procedures for Silent Aircraft," AIAA Paper No. 2007-451.

[3] Lockard, D. P., and Lilley, G. M., 2004, "The Airframe Noise Reduction Challenge," NASA Langley Research Center, Hampton, VA, Technical Report No. 213013.

[4] Antoine, N. E., and Kroo, I. M., 2004, "Aircraft Optimization for Minimal Environmental Impact," J. Aircr., 41(4), pp. 790–797.

[5] Filippone, A., 2007, "Steep-Descent Maneuver of Transport Aircraft," J. Aircr., 44(5), pp. 1727–1739.

[6] Clarke, J.-P. B., Ho, N. T., Ren, L., Brown, J. A., Elmer, K. R., Zou, K., Hunting, C., McGregor, D. L., Shivashankara, B. N., Tong, K.-O., Warren, A. W., and Wat, J. K., 2004, "Continuous Descent Approach: Design and Flight Test for Louisville International Airport," J. Aircr., 41(5), pp. 1054–1066.

[7] Reynolds, T. R., Ren, L., Clarke, J.-P., Burke, A., and Green, M., 2005, "History, Development, and Analysis of Noise Abatement Arrival Procedures for U.K. Airports," AIAA Paper No. 2005-7395.

[8] Heathrow Airport, 2015, "Heathrow's Blueprint for Noise Reduction: Ten Practical Steps to Cut Noise by Summer 2015," Heathrow Airport, Longford, UK.

[9] Lutz, T., and Wieser, T., 2006, "Heading for the City: A318 Steep Approach Development," The International Federation of Air Line Pilots' Associations, Montreal, QC, Canada.

[10] Anil Mertol, B., 2008, "An Airbrake Design Methodology for Steep Approaches," New Results in Numerical and Experimental Fluid Mechanics, Vol. 6, Springer, Berlin, pp. 1–8.

[11] Jung, U., and Brietsamter, C., 2010, "Aerodynamic Wake Investigations of High-Lift Transport Aircraft With Deployed Spoilers," 27th International Congress of the Aeronautical Sciences (ICAS), Nice, France, Sept. 19–24, Paper No. ICAS2010-P2.23.

[12] Jung, U., and Brietsamter, C., 2012, "Aerodynamics of Multifunctional Transport Aircraft Devices," J. Aircr., 49(6), pp. 1755–1764.

[13] Business & Commercial Aviation, 2015, "Pilatus Designs the PC-24 to Do Everything," Aviation Week Network, Arlington, VA, accessed Oct. 26, 2015, http://aviationweek.com/business-aviation/pilatus-designing-pc-24-do-everything

[14] GPO, 2007, "Landing Climb: All Engines Operative," U.S. Government Publishing Office, Washington, DC.

[15] GPO, 2007, "Climb: One Engine Inoperative," U.S. Government Publishing Office, Washington, DC.

[16] Business & Commercial Aviation, 2016, "Preparing for Descent During Low Workload Phases of Cruise Prevents Poor Performance," Aviation Week Network, Arlington, VA, accessed Jan. 28, 2016, http://aviationweek.com/business-aviation/preparing-descent-during-low-workload-phases-cruise-prevents-poor-performance

[17] Shah, P. N., Mobed, D. D., and Spakovszky, Z. S., 2007, "Engine Air-Brakes for Quiet Air Transport," AIAA Paper No. 2007-1033.

[18] Shah, P. N., Mobed, D. D., and Spakovszky, Z. S., 2010, "A Novel Turbomachinery Air-Brake Concept for Quiet Aircraft," ASME J. Turbomach., 132(4), p. 041002.

[19] Shah, P. N., Robinson, A., Price, A., and Spakovszky, Z., 2010, "Aeroacoustics of Drag-Generating Swirling Exhaust Flows," AIAA J., 48(4), pp. 719–737.

[20] Shah, P., Mobed, D. D., and Spakovszky, S. S., 2013, "Drag Management in High Bypass Turbofan Nozzles for Quiet Approach Applications," ASME J. Turbomach., 136(2), p. 021009.

[21] Shah, P., and Spakovszky, Z., 2011, "Aeroacoustics of Swirling Exhaust Flows in High Bypass Ratio Turbofan Nozzles for Drag Management Applications," AIAA Paper No. 2011-2903.